ACS APPLIED MATERIALS & INTERFACES

Research Article

www.acsami.org

Magnetic Bioinspired Hybrid Nanostructured Collagen–Hydroxyapatite Scaffolds Supporting Cell Proliferation and Tuning Regenerative Process

Anna Tampieri,*[,†] Michele Iafisco,[†] Monica Sandri,[†] Silvia Panseri,[†] Carla Cunha,[†,‡] Simone Sprio,[†] Elisa Savini,[†] Marc Uhlarz,[§] and Thomas Herrmannsdörfer[§]

[†]Institute of Science and Technology for Ceramics (ISTEC), National Research Council (CNR), Via Granarolo 64, 48018 Faenza, Italy

[‡]INEB—Instituto de Engenharia Biomédica, University of Porto, Rua do Campo Alegre 823, 4150-180 Porto, Portugal

[§]Dresden High Magnetic Field Laboratory, Helmholtz-Zentrum Dresden-Rossendorf (HZDR), 01314 Dresden, Germany

Supporting Information

ABSTRACT: A bioinspired mineralization process was applied to develop biomimetic hybrid scaffolds made of (Fe^{2+}/Fe^{3+})-doped hydroxyapatite nanocrystals nucleated on self-assembling collagen fibers and endowed with super-paramagnetic properties, minimizing the formation of potentially cytotoxic magnetic phases such as magnetite or other iron oxide phases. Magnetic composites were prepared at different temperatures, and the effect of this parameter on the reaction yield in terms of mineralization degree, morphology, degradation, and magnetization was investigated. The influence of scaffold properties on cells was evaluated by seeding human osteoblast-like cells on magnetic and nonmagnetic materials, and differences in terms of viability, adhesion, and proliferation were studied. The synthesis temperature affects mainly the chemical–physical features of the mineral phase of the composites influencing the degradation, the microstructure, and the magnetization values of the entire scaffold and its biological performance. In vitro investigations indicated the biocompatibility of the materials and that the magnetization of the super-paramagnetic scaffolds, induced applying an external static magnetic field, improved cell proliferation in comparison to the nonmagnetic scaffold.

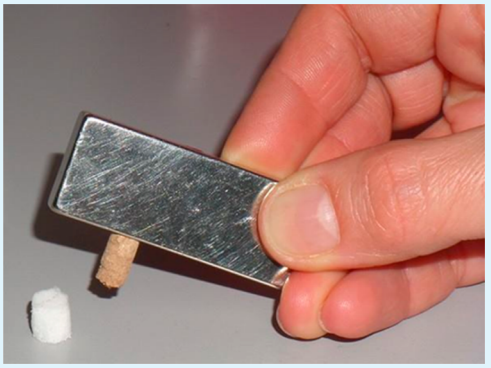

KEYWORDS: *bone scaffolds, magnetic materials, tissue engineering, collagen, magnetic nanoparticles*

INTRODUCTION

In the last few decades, tissue engineering has emerged as a promising multidisciplinary approach for the repair and regeneration of damaged bone tissue.[1,2] This approach combines the application of cells capable of osteogenic activity and osteoinductive signal molecules with an appropriate scaffold.[3] In the last years, a lot of attention has been focused on the preparation of materials based on calcium phosphate (CaP) bioceramics such as hydroxyapatite (HA) and tricalcium phosphates (TCP), which are by themselves osteoconductive.[4,5] More recently, new biomaterials in form of hybrid composites constituted by apatitic phase nucleated on organic template have been developed.[6,7] Such composites have demonstrated enhanced cell proliferation and osteoinductivity and high regenerative potential, as a result of the peculiar characteristics of the inorganic phase that grows in a confined fashion increasing the biomimetism with the mineral component of the natural bone.[8,9] In particular, the use of collagen (Coll) as polymeric template for biomineralization processes and for the activation of self-regulating mechanisms, inducing the formation of biomimetic nanocomposites, has been studied and experimented earlier.[10−12]

In spite of the outstanding regenerative properties of the biohybrid HA/Coll composites, the possibility to completely regenerate hard connective tissues is limited by the size of the lesions.[13] In fact, the regeneration of extended bone portions must be assisted by substantial angiogenesis, and in this respect, it has been demonstrated that in absence of a continuous and prolonged stimulation, the cell colonization of bone implants is limited to few millimeters from the bone-implant interface.[13] A low cell penetration depth results in the formation of necrotic areas in the inner parts of the scaffold and insufficient functionality and stability of the newly formed bone.[13] To stimulate osteogenesis and angiogenesis, biologics such as bone morphogenetic proteins (BMPs) and vascular endothelial growth factors (VEGFs) could be used;[14] however, their half-life in the human body is very short, and this hampers both the

Received: April 11, 2014
Accepted: September 3, 2014
Published: September 3, 2014

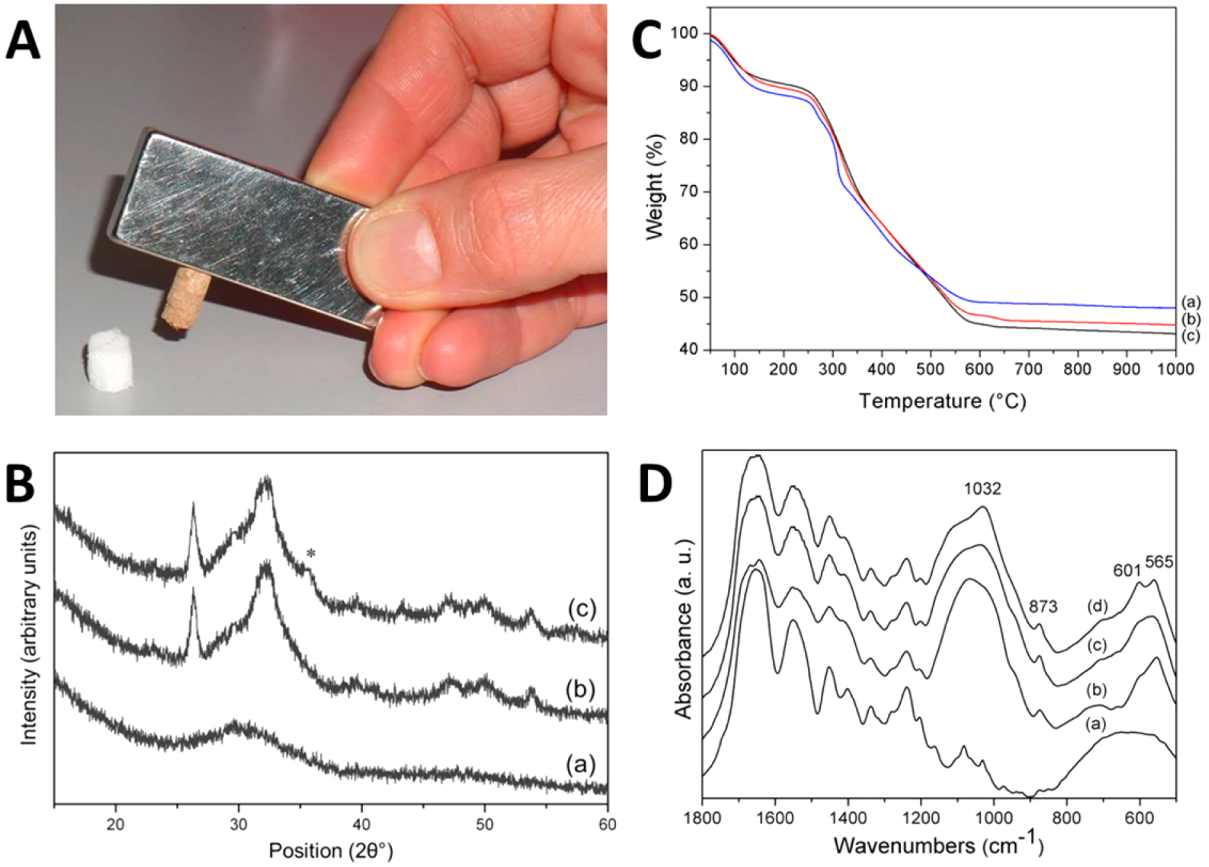

Figure 1. (A) Photograph of magnetic FeHA/Coll (brownish scaffold attached to the magnet) and nonmagnetic HA/Coll (white scaffold) scaffolds. (B) XRD patterns of (a) FeHA/Coll25, (b) FeHA/Coll40, and (c) FeHA/Coll50; the peak identified by * corresponds to magnetite. (C) TGA curves of (a) FeHA/Coll25, (b) FeHA/Coll40, and (c) FeHA/Coll50. (D) FT-IR spectra of (a) Coll, (b) FeHA/Coll25, (c) FeHA/Coll40, and (d) FeHA/Coll50.

systemic approach and the local administration.[15] To solve this problem, it is necessary to develop new solutions that associate the presence of biomimetic and osteoconductive scaffolds with prolonged and controlled biochemical stimulations.

To this aim, the preparation of magnetic scaffolds which mimic the complexity of bone structure from the macro- to the molecular scale and which enable an activation of cell adhesion and proliferation under the stimulus of magnetic field can be an appealing solution. In fact, it has been previously demonstrated that weak magnetic or pulsed electromagnetic fields are effective stimuli that promoted bone fracture healing, spinal fusion and bone ingrowth in animal models.[16−20] Strong static magnetic fields between 5 to 10 T were reported to have the ability to regulate in vitro and in vivo the orientation of protein matrices and cells along the field lines.[21−23] Therefore, the association of magnetic stimulation and suitable biochemical agents could lead to more efficient treatments for the regeneration of extended bone and osteochondral regions.[24]

Recently, several works have demonstrated that magnetic nanoparticles (MNPs) embedded in polymeric or inorganic scaffolds have a positive effect on the osteoinduction with and without application of external magnetic force. In particular, it was reported that the introduction of MNPs into CaP bioceramics promoted bone formation and growth in vitro and in vivo[25,26] and the addition of MNPs in fibrous polymeric scaffolds induced higher cell proliferation and faster differentiation in osteoblasts in vitro and enhanced osteogenesis and new bone tissue formation in an animal model; moreover, their magnetic behavior can allow to label the scaffold to be visualized in vivo by magnetic resonance imaging (MRI).[27−32]

In this view, magnetic scaffolds might offer great potential in bone regenerative medicine particularly if it was possible to synthesize a biomimetic biodegradable magnetic phase to replace magnetite and the other iron oxide phases (maghemite, etc.). In fact, the long-term cytotoxic effects of the iron oxides in the human body are not yet completely assessed and nowadays their use is becoming a critical issue due to their accumulation in soft tissues and organs such as liver and kidney.[33,34]

Recently, Tampieri et al. developed a new biocompatible and bioresorbable superparamagnetic-like phase by doping HA with Fe^{2+}/Fe^{3+} ions (FeHA).[35] The in vitro study revealed that FeHA nanoparticles do not reduce cell viability and do at the same time enhance cell proliferation compared to HA particles. This effect was even significantly increased when a magnetic field was applied.[36] Moreover, a pilot animal study of bone repair (a rabbit critical bone defect model) demonstrated the in vivo biocompatibility and biodegradability of FeHA.[36] FeHA nanoparticles also have been used recently to synthesize magnetic hybrid inorganic−polymeric composites in the form of films and hollow micro-nano spheres.[37−39]

In this work, FeHA was directly nucleated on self-assembling Coll (type I) fibers using a biologically inspired mineralization process.[7,40] Magnetic hybrid FeHA/Coll composites were prepared at different temperatures and the effect of this parameter has been correlated to the reaction yield in terms of

mineralization degree and magnetization. The influence of scaffold properties on cellular response was investigated by seeding MG63 human osteoblast-like cells both on magnetic and nonmagnetic scaffolds, and differences on cell behavior were analyzed.

EXPERIMENTAL SECTION

Synthesis of the Magnetic Hybrid Composites. Telopeptides-free type I Coll from horse tendon was supplied by Opocrin SpA, (Corlo di Formigine (MO), Italy) in the form of gel (1 wt % of Coll in acetic solution buffered at pH = 3.5). A well-established biologically inspired process of pH-driven self-assembly of Coll fibrils and simultaneous mineralization with FeHA phase was applied.[7] In detail, a basic suspension was prepared mixing three aqueous solutions: (i) 2.71 g of $Ca(OH)_2$ (Sigma-Aldrich ≥95 wt % pure) dissolved in 500 mL; (ii) 0.689 g of $FeCl_2{\cdot}4H_2O$ (Sigma-Aldrich, ≥ 99 wt % pure) dissolved in 25 mL; and (iii) 0.574 g of $FeCl_3{\cdot}6H_2O$ (Sigma-Aldrich, ≥ 98 wt % pure) dissolved in 25 mL (total Fe = 6.2 wt %). A defined amount of iron salts was set to obtain the Fe/Ca theoretical molar ratio equal to 0.16 in the magnetic CaP phase. To avoid oxidation of Fe^{2+} to Fe^{3+} by the acetic acid of Coll, 150 g of Coll gel were fibrated with NaOH solution (0.1 M) added drop by drop up to pH 5.5 and extensively washed with ultrapure water by centrifugation. Then, the assembled Coll was resuspended adding 260 mL of H_3PO_4 (0.08 M) (Sigma-Aldrich, ≥ 85 wt % pure) and dropped into the basic suspension to synthesize the hybrid composite with the FeHA/Coll nominal ratio of 70/30 wt % mimicking the bone composition.[41] The dropwise addition procedure was carried out under stirring and heating, assuring a slow pH decrease. The reaction product was kept in suspension by continuous stirring and heating for 2 h after the neutralization reaction. The preparation of the magnetic hybrid FeHA/Coll composites was carried out at different temperatures, T = 25, 40, and 50 °C, and the obtained composites are hereafter labeled as FeHA/Coll25, FeHA/Coll40, and FeHA/Coll50.

After the mineralization process, materials were filtered by the use of a metallic sieve (50 μm) to separate the inorganic phases not attached to Coll and the denaturated fibers (both passed through the sieve) from the mineralized fibrous fraction having dimensions higher than 50 μm. The latter part of the material was recovered and poured into plastic molds for the preparation of the scaffolds. A controlled freeze-drying process was applied setting the precise cooling temperature (−40 °C) and heating ramp (2 °C min^{-1} up to −5 and 1 °C min^{-1} up to 25 °C) at p = 0.1 mbar to achieve dried porous scaffolds. The products were then stabilized using 1,4-butanediol diglycidyl ether (BDDGE) in aqueous solution (2.5 mM) as cross-linking agent. The soaking procedure was carried out setting a BDDGE/Coll ratio equal to 1 wt % and lasted 24 h at 25 °C.[42] The samples were then washed several times with ultrapure water to remove the unreacted BDDGE and freeze-dried again with the same conditions used before. FeHA/Coll scaffolds displayed a brownish color in comparison to the white color of nonmagnetic HA/Coll scaffold (Figure 1A).

Nonmagnetic scaffolds made of pure Coll and HA/Coll (60/40 wt %) for use as reference materials were prepared according to the syntheses previously described.[8]

Physical−Chemical, Morphological, and Magnetic Characterization. Quantitative determination of Fe, Ca, and P was carried out by the use of an inductively coupled plasma−atomic emission spectrometer (ICP-OES) Liberty 200 (Varian, Clayton South, Australia). Samples were dissolved in 1 wt % HNO_3 (Aldrich, 65 wt % pure) prior to the analysis.

The infrared spectra were collected in the wavelength ranging from 400 to 4000 cm^{-1} with 2 cm^{-1} of resolution with a Nicolet 380 FT-IR spectrometer (Thermo Fisher Scientific Inc., Waltham, MA). The sample (~2 mg) was mixed with 100 mg of anhydrous KBr and the powder pressed at 8000 psi into 7 mm diameter discs.

The X-ray diffraction (XRD) patterns of the samples were recorded in the 2θ range from 10 to 60° with a step size (2θ) of 0.02° and a counting time of 1 s with a D8 Advance Diffractometer (Bruker, Karlsruhe, Germany) equipped with a Lynx-eye position sensitive detector using Cu Kα radiation (λ = 1.54178 Å) generated at 40 kV and 40 mA.

Scanning electron microscopy (SEM) was used for the morphological characterization employing a Stereoscan 360 (Cambridge Instruments, U.K.) equipped with a secondary electron detector and an accelerating voltage of 15 kV. For a more detailed morphological investigation, transmission electron microscopy (TEM) analysis also was performed by a JEM-3010 (Jeol Ltd., Japan), operated at 300 kV. Further experimental details are reported in the Supporting Information. Selected area electron diffraction (SAED) was carried out on the mineral phase during the TEM analyses.

The thermal properties of the samples were measured using STA 449/C Jupiter (Netzsch, Germany). Simultaneous thermal gravimetric analysis (TGA) and differential scanning calorimetry (DSC) were carried out in alumina crucibles from room temperature to 1200 °C at a heating rate of 10 °C/min in nitrogen flow. The weight of the samples was approximately 10 mg.

Magnetization measurements were performed in a Superconducting Quantum Interference Device (SQUID) magnetometer (Quantum Design, San Diego, CA), operating from T = 1.8−350 K with a maximum applied magnetic field of H = 7T. About 20 mg of the scaffolds were measured in a magnetic field cycle from −2T to +7T at T = 310 K (close to the physiological temperature) to estimate the magnetization vs magnetic field (M vs H) curve.

In Vitro Degradation. Scaffolds were immersed into fetal bovine serum (FBS) (PAA Laboratories GmbH) at 37 °C up to 21 days with a weight-to-volume ration of 30 mg/mL, and the solution was refreshed every day. At scheduled times scaffolds were removed, gently rinsed with ultrapure water, dried in vacuum overnight, and weighted. The degradability of scaffolds was estimated from the rate of weight loss (W_L) using eq 1

$$W_L = \frac{(W_0 - W_t)}{W_0} 100 \quad (1)$$

where W_0 and W_t are the dry weights of the initial and the degraded specimens at different immersion times, respectively.

In Vitro Cell Culture Analysis. MG63 Human Osteosarcoma cell line was purchased from Lonza (Italy) and cultured in Dulbecco Modified Eagle's Medium (DMEM, PAA, Austria), containing penicillin/streptomycin (100 U/mL/100 μg/mL) supplemented with 10% fetal bovine serum and kept at 37 °C in an atmosphere of 5% CO_2. Cells were detached from culture flasks by trypsinization and were centrifuged; cell number and viability were assessed with trypan-blue dye exclusion test. HA/Coll, FeHA/Coll25, FeHA/Coll40, and FeHA/Coll50 scaffolds, 8.00 mm diameter and 3.00 mm high, were sterilized by 25 kGy γ-ray radiation prior to use. Samples were placed one per well in a 24-well plate and presoaked in culture medium. Each scaffold was seeded by carefully dropping 30 μL of cell suspension (7.5 × 10^4 cells) onto the upper scaffold surface, allowing cell attachment for 15 min, before addition into each well of 1.5 mL of cell culture medium supplemented with 10 μg/mL ascorbic acid and 5 mM β-glycerophosphate for osteoblast activation. After a 6 h incubation step, each scaffold was carefully placed in a new 24-well plate to eliminate any contribution of remnant cells from the cell suspension that might grow into the scaffold from its bottom surface. The medium was changed every 2 days. Osteoblast proliferation, cell viability, and morphology were analyzed after 1, 3, and 7 days. Moreover, osteoblast markers expression was investigated at day 7. All cell-handling procedures were performed in a sterile laminar flow hood. All cell-culture incubation steps were performed at 37 °C with 5% CO_2.

Cell Viability Assay. Live/Dead assay kit (Invitrogen) was performed according to manufacturer's instructions. Briefly, scaffolds were washed with 1× PBS for 5 min and incubated with Calcein acetoxymethyl (Calcein AM) 2 μM plus Ethidium homodimer-1 (EthD-1) 4 μM for 15 min at 37 °C in the dark. Samples were rinsed in 1× PBS, finely cut with a scalpel in order to examine also the internal surface. Images were acquired by an inverted Ti-E

Table 1. Chemical−Physical Features of the FeHA/Coll Hybrid Composites

	(Ca + Fe)/P	Ca/P	Fe/Ca	Fe (wt %)[a]	magnetization at 7T (emu/g)[b]
FeHA/Coll25	1.94 ± 0.04	1.71 ± 0.03	0.14 ± 0.01	2.97 ± 0.06	0.091 ± 0.004
FeHA/Coll40	1.70 ± 0.03	1.43 ± 0.04	0.19 ± 0.03	3.83 ± 0.12	0.182 ± 0.009
FeHA/Coll50	1.70 ± 0.06	1.38 ± 0.06	0.23 ± 0.03	4.43 ± 0.21	1.103 ± 0.055

[a]Calculated with respect to the mass of the inorganic phase. [b]Calculated with respect to the total mass of the scaffolds.

fluorescence microscope (Nikon). One sample per time point was analyzed.

Cell Proliferation Assay. MTT reagent (3-(4,5-dimethylthiazol-2-yl)-2,5-diphenyltetrazolium bromide) (Invitrogen) was prepared at 5 mg/mL in 1x PBS. Scaffolds were incubated with the MTT reagent 1:10 for 2 h at 37 °C. Scaffolds were transferred in 1.5 mL microcentrifuge tubes and incubated with 1 mL of dimethyl sulfoxide for 15 min, then homogenized with polypropylene pestles and centrifuged for 1 min at 1000 rpm. The metabolically active cells react with the tetrazolium salt in the MTT reagent to produce a formazan dye and it was detected at λ_{max} of 570 nm, using a Multiskan FC Microplate Photometer (Thermo Scientific). The experiments were carried out either with or without applying a static magnetic field (SMF) of 320 mT (MagnetoFACTOR-24, Chemicell, Germany). Three samples per time point were analyzed.

Cell Morphology Evaluation. Two samples for each time point were used for actin immunofluorescence and SEM analysis, respectively. In order to visualize actin filaments, samples were subjected to FITC-conjugated phalloidin immunocytochemistry followed by DAPI staining and visualized with an Inverted Ti-E fluorescence microscope (Nikon). For SEM analysis, after fixation in 2.5% glutaraldehyde, samples were sputter-coated with gold and examined using Stereoscan 360 Scanning Electron Microscope (Cambridge Instruments, U.K.). More details are reported in the Supporting Information.

Quantitative Real-Time Polymerase Chain Reaction (qPCR). Gene expression was quantified for type I Coll, α-1 (Col1A1), Runt-related transcription factor 2 (RUNX2), and alkaline phosphatase (ALP) for FeHA/Coll25 and HA/Coll scaffolds at day 7. More details are reported in Supporting Information.

Statistical Analysis. For degradation (n = 5) and cell proliferation (n = 3), results were expressed as mean value ± standard deviation and were plotted on a graph. For the analysis among the groups two-way ANOVA, followed by Bonferroni's posthoc test was used. All statistical analysis made use of the GraphPad Prism software (version 5.0), with α = 0.05.

2. RESULTS

Characterization of the Magnetic Hybrid Composites. XRD pattern of the hybrid composites synthesized at 25 °C displayed the typical shape ascribable to a CaP phase without long-range periodic regularity close to an amorphous one,[43] while those of the scaffolds prepared at higher temperatures exhibited the characteristic broad diffraction peaks of nanocrystalline apatite with very low coherent length[5] (Figure 1B), since the interaction with the organic template confined the mineral nuclei growth at the nanoscale. Moreover, it is well-known that the introduction of foreign ions yields destabilization of apatite lattice resulting in a further reduction of crystalline degree.[44] Similar XRD profiles were previously found analyzing HA/Coll and MgHA/Coll composites prepared with the same approach.[7,8] Due to its amorphous nature, the CaP phase doped with Fe synthesized at 25 °C should not be identified as HA, but for the sake of simplicity, we will use in the manuscript the code FeHA. In the FeHA/Coll40 and FeHA/Coll50 scaffolds, a preferential orientation along the c-axis of the apatite was detected as demonstrated by the high resolution and intensity of the diffraction peak at 2θ = 26° attributed to the (002) plane. This preferential orientation can be due to the fact that the FeHA nuclei grew in tight contact with the fibers with their c-axis preferentially oriented parallel to the direction of Coll fibers orientation. The low resolution of the diffraction patterns did not allow the accurate evaluation of crystallographic parameters preventing any comparison with lattice distortion detected in the previously synthesized FeHA.[35] The XRD spectra of FeHA/Coll50 displayed a peak at $2\theta \approx 36°$, which can be attributed to the presence of magnetite since its formation is favored at temperatures above 40 °C.[45] The careful quantification of magnetite amount by Rietveld refinement was difficult due to the very low crystallinity degree of the inorganic phases, but according to the relative intensity of the magnetite peak ($2\theta \approx 36°$) with respect to those of apatite, it can be estimated to be less than 2 wt %.[35]

TGA analyses were carried out to evaluate the mineralization extent in the composites (Figure 1C). The hybrid composites had a nominal composition FeHA/Coll of 70/30 wt %, while the amount of the inorganic phase was found to be in the range 55−60 wt %. This value was almost similar in all the composites with a slightly greater amount of the mineral phase in the scaffolds synthesized at 25 °C (2−3 wt %). The discrepancy between the nominal and the real compositions of the scaffolds can be assigned to the reaction yield, which does not reach 100%, in line with the previous works where HA/Coll and MgHA/Coll composites where prepared.[7,8] The higher amount of mineral phase in the composite prepared at 25 °C is probably due to the fact that at low temperature the availability of the nucleation sites on collagen is higher. At higher temperature the partial denaturation of the polymer as well as the increase in its nanoassembly, driven by hydrophilic interactions, trigger to a reduction in the Ca and Fe ions binding.[46,47]

The chemical features of the nucleated mineral phase evaluated by ICP-OES analysis are reported in Table 1. The (Ca + Fe)/P molar ratio of FeHA/Coll25 was higher than the theoretical Ca/P ratio (1.67) for HA due to the amorphous nature of the mineral phase as detected from XRD analysis and the resulting incorporation of Fe ions in nonordered positions. In the case of FeHA/Coll40 and FeHA/Coll50 composites, the (Ca + Fe)/P molar ratios were very close to 1.67, confirming the depletion of Ca and the possible replacement with Fe ions. The total Fe wt % of the FeHA/Coll25 scaffold was about half of the starting nominal concentration, and it was significantly lower than the Fe wt % of the samples synthesized at higher temperature. The higher quantity of the total Fe wt % in the FeHA/Coll50 composite is consistent with the fact that the temperature favored the entrance of iron instead of calcium into the crystal lattice[35] and with the formation of a small amount of magnetite as demonstrated by XRD.

Fourier transform infrared (FT-IR) spectra of the hybrid composites confirmed the presence of the CaP phase nucleated on the protein fibers (Figure 1D). In particular, the typical bands of CaP at about 1032, 565, and 601 cm^{-1} were clearly

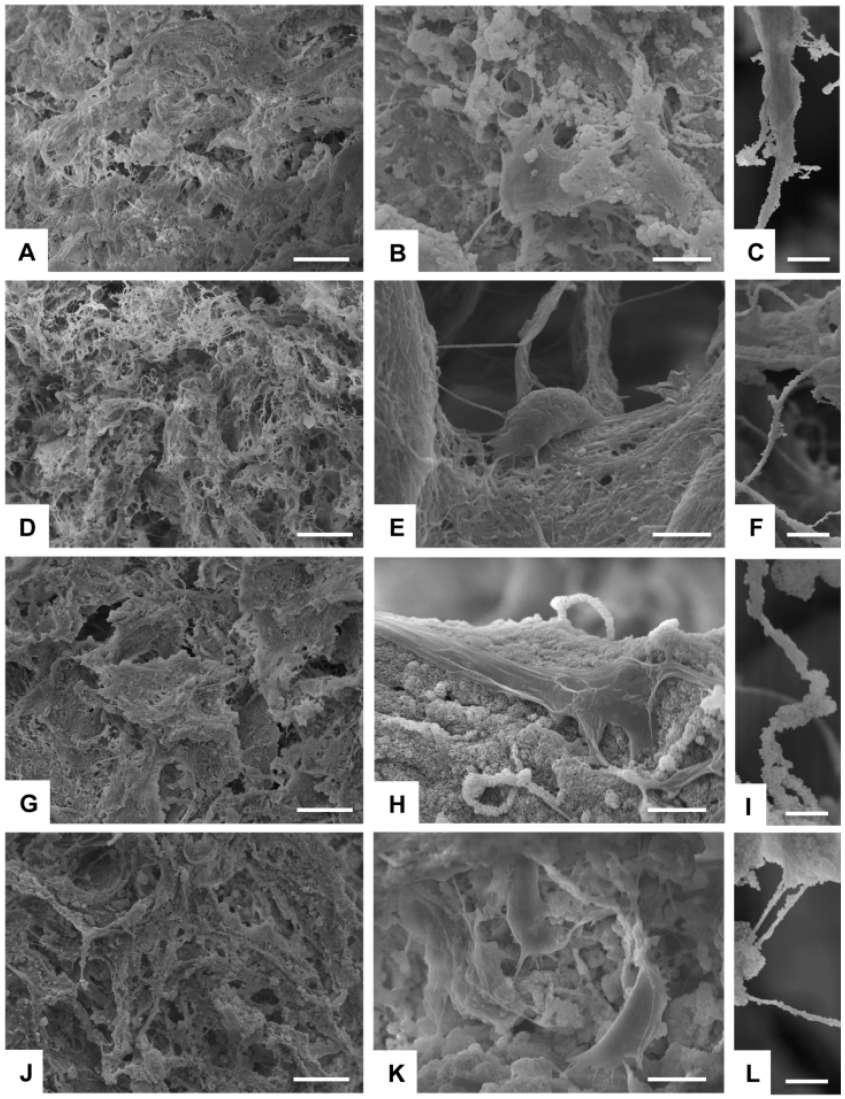

Figure 2. SEM images of (A, B, C) HA/Coll, (D, E, F) FeHA/Coll25, (G, H, I) FeHA/Coll40, and (J,K,L) FeHA/Coll50. (A, D, G, J) Morphology of the hybrid scaffolds. (B, E, H, K) Morphology of cell-seeded scaffolds at day 1. (C, F, I, L) Detailed morphology of the mineral phase of the hybrid scaffolds. Scale bars: (A, D, G, J) 100 μm; (B,E,H,K) 10 μm; (C, F, I, L) 5 μm.

visible in comparison with the spectrum of not-mineralized collagen scaffolds.[48] The resolution of these bands increased as a function of the temperature due to the different CaP phases crystallized at different temperatures (amorphous CaP at 25 °C and apatite at 40 and 50 °C). Moreover, the comparison of the FT-IR spectra of FeHA/Coll40 and FeHA/Coll50 showed enhanced resolution of the phosphate bands for this latter sample (clearly visible in the bands at 565 and 601 cm^{-1} ascribed to the triply degenerated bending mode of PO_4) demonstrating a slightly enhanced crystallinity degree of the apatitic phase caused by the temperature. The presence of the band at 873 cm^{-1} indicated that carbonate group substituted phosphate group in the FeHA phase nucleated onto the collagen fibers. The spontaneous carbonation of FeHA occurred only to the B position (carbonate replacing phosphate), in compliance with the chemical composition of biological apatite.[5]

SEM images of the HA/Coll and FeHA/Coll scaffolds are reported in Figure 2. FeHA/Coll25 morphology (Figure 2D, F) appeared formed by very small nanocrystals closely bound to the collagen fibers giving to the material a porous architecture with a network of micro-macro porosity. Higher synthesis temperatures (FeHA/Coll40 (Figure 2I) and FeHA/Coll50 (Figure 2L)) leaded the growing of an external layer of bigger apatite crystals with a plate-like morphology increasing the thickness of the collagen fibers and reducing the final porosity of the composites after freeze-drying (Figure 2G,J). The comparison between the morphologies of the HA/Coll (Figure 2A,C) and the FeHA/Coll25 (Figure 2D, F) composites that were synthesized at the same temperature, underlined more disjointed structures in the Fe-doped composites. This effect is probably due to the affinity of Fe ions for collagen[49] preventing the fiber−fiber interaction and destabilizing the assembly of collagenous matrix. This reaction can provoke a fast saturation of the carboxylic sites and induce the formation of a big number of nuclei of well-linked and homogeneously distributed FeHA reducing the organization of the fibrous matrix.

The denaturation temperature (T_d) of the mineralized collagen with HA and FeHA at different temperatures calculated by DSC analyses (Supporting Information Figure S1) indicated that the iron as well as the new FeHA phase formed at higher synthesis temperature decrease the thermal

stability of the cross-linked scaffolds. The T_d of the FeHA/Coll scaffolds are in the range 85−92 °C similarly to other cross-linked mineralized collagen scaffolds reported in scientific literature[50,51] and sensibly higher than the magnetic collagen scaffolds labeling with iron oxide nanoparticle[32] demonstrating the distinctive effect of the biomineralization approach used in this work to prepare functional materials.

A detailed morphological analysis of the apatitic nanocrystals and their interaction with the collagen fibers was evaluated by TEM analyses (Figure 3). Low magnification images provide

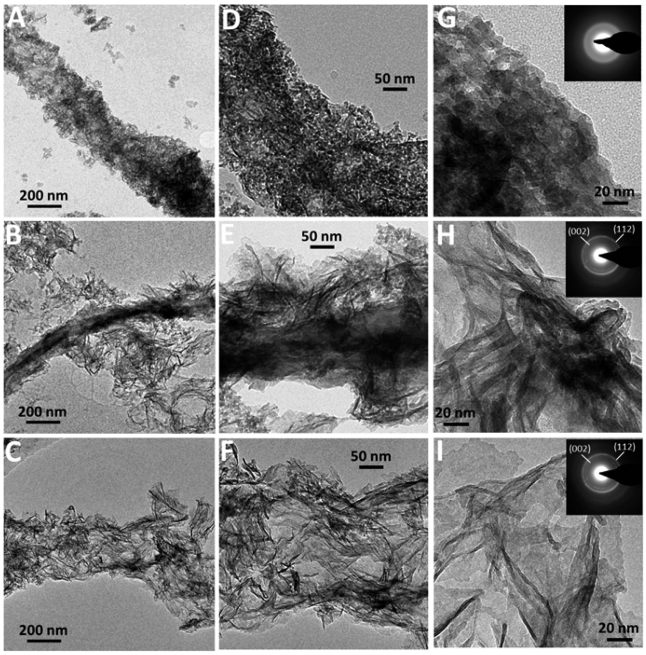

Figure 3. TEM images representative (i) of the assembly of FeHA nanoparticles in contact with the collagen fibers ((A) FeHA/Coll25, (B) FeHA/Coll40, (C) FeHA/Coll50; (ii) of the interface between collagen and the mineral phase ((D) FeHA/Coll25, (E) FeHA/Coll40, (F) FeHA/Coll50) and (iii) of the external border of the FeHA nanoparticles in contact with the collagen fibers ((G) FeHA/Coll25, (H) FeHA/Coll40, (I) FeHA/Coll50). Insets: corresponding SAED patterns. Scale bars: (A−C) 200 nm, (D−F) 50 nm, (G−I) 20 nm.

evidence of the close assembly of the apatitic crystals resulting from the stacking of FeHA nanoparticles on a "primary layer" grown in close contact and merged with the surface of the collagen matrix (Figure 3A−F). The morphology of the FeHA particles appeared different in dependence on the synthesis temperature. As can be seen clearly from the high-magnification images of the external border of apatite assembled on the collagen fibers, the particles of the FeHA/Coll25 appeared as round-shape aggregates of about 20−30 nm and the diffusive SAED pattern (inset in Figure 3G) confirmed their amorphous nature. On the contrary the particles of the FeHA/Coll40 and FeHA/Coll50 scaffolds (Figure 3H,I) produced in both cases two different projections on the image plane, one resulting in more plate-like shapes approximately 100−120 nm (length) by 55−75 nm (width) in size, characterized by a weak contrast, and the other in needle-like shapes of approximately 100−120 nm (length) by 5−10 nm (width), appearing significantly darker. On the base of the mass−thickness contrast mechanism[52] the latter might then correspond to a "side view" of the particles with plate-like morphology. The preferential orientation of the FeHA nanocrystals along their *c*-axis (more evident in the FeHA/Coll40) is in agreement with the XRD analyses. The SAED patterns collected for the inorganic particles of the FeHA/Coll40 and FeHA/Coll50 scaffolds (insets in Figure 3H, I) were similar to those reported for nanocrystalline apatites characterized by diffuse rings at *d*-spacing equal to 3.44 and 2.75 Å corresponding to the (002) and (112) crystallographic planes of HA, respectively (ASTM Card File No. 9-432).[48,53] It is worth to notice that for both materials no particles with significant different morphology, likely due to separated iron oxide phases, were observed.

Magnetic Properties. The magnetic properties of the FeHA/Coll scaffolds are reported in Figure 4 and Table 1. The magnetization curves at T = 310 K (black curves) can be decomposed into two components: the background (blue lines), increasing linearly with the field which is typical for paramagnetism far away from saturation, can probably be assigned to collagen, and one component following a Brillouin function (red curves) due to the super-paramagnetism of FeHA. The paramagnetic background was of comparable magnitude for all the scaffolds, in agreement with the similar amounts of collagen in the samples. The amorphous nature and the short-range periodic regularity of the FeHA nucleated on the collagen at 25 °C caused a poor coordination level of the Fe ions, reflecting in a low magnetization value (0.091 emu/g at 7T) (Figure 4A). Higher magnetization values were measured for the scaffolds prepared at higher temperatures (Figure 4B, C), indicating that increase of the temperature facilitates the substitution and the coordination level of the Fe ions in the lattice, as also confirmed by quantitative chemical analysis. Moreover, the very high magnetization value of FeHA/Coll50 in comparison with FeHA/Coll40 cannot be justified only with the presence of magnetite but probably it can be explained on the basis of an additional contribution due to the formation of a new magnetic phase, as confirmed by the higher Fe ions incorporation.

In Vitro Degradation. The scaffolds degradation was evaluated measuring their weight loss in FBS as a function of time (Figure 5). The degradation rate of the magnetic composites was similar up to 14 days of immersion, while the weight loss of FeHA/Coll25 was higher than those of FeHA/Coll40 and FeHA/Coll50 from 14 days onward. This finding can be due to the different mineral phase nucleated on the FeHA/Coll25 (i.e., amorphous CaP is more degradable than nanocrystalline apatite[54]) and to the increase of the thickness of the collagen fibers in the FeHA/Coll40 and FeHA/Coll50 as evaluated by SEM analyses. The increase of the fibers thickness reduced the total surface area of the scaffolds decreasing the open porosity and the amount of material in contact with the physiological fluid, thus the degradation rate. The weight losses of the cross-linked collagen scaffolds immersed in phosphate buffered saline (PBS) at 37 °C reported in other works[55] are similar to those obtained for the cross-linked magnetic scaffolds synthesized in this work. It should be noted that this degradation study was carried out in absence of enzymes and cells and therefore cannot be predictive of the actual resorption time in vivo.

In Vitro Analysis of the Magnetic Hybrid Composites. *No Magnetic Field Application.* Cell viability assay was performed for each time point without magnetic field application in order to evaluate the live and dead cells of the magnetic FeHA/Coll scaffolds. All the groups demonstrated high cell viability representing good biocompatibility, with HA/

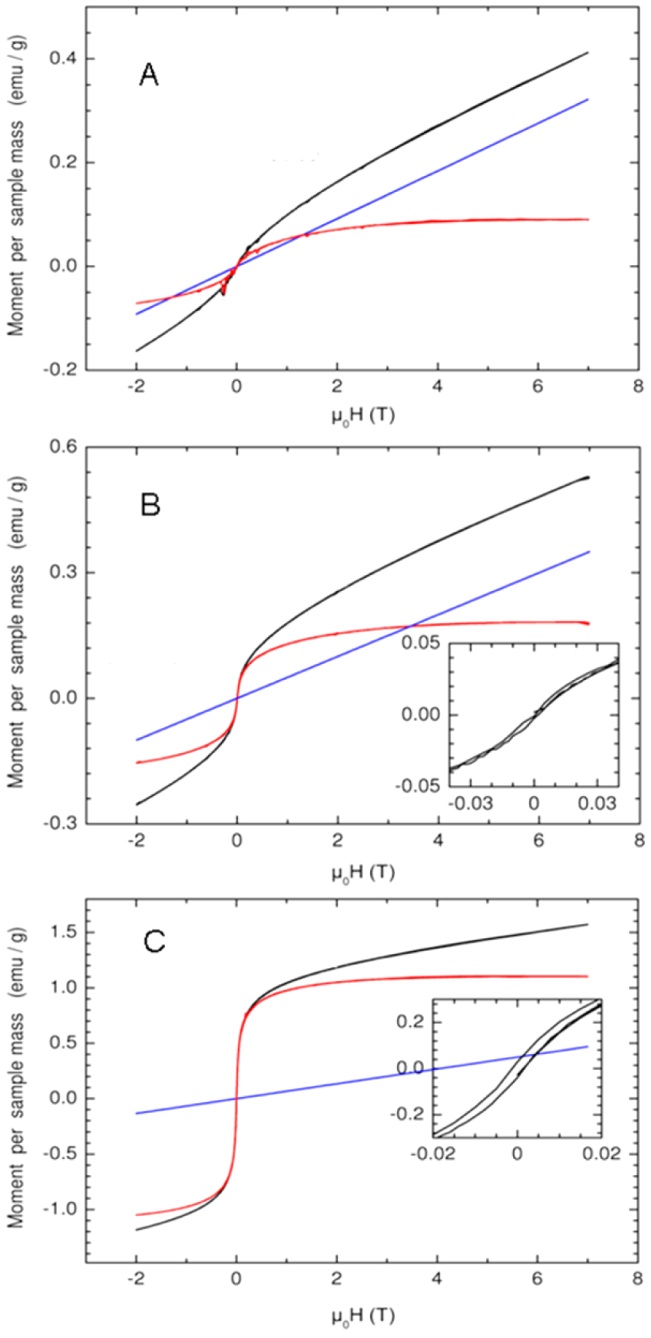

Figure 4. Magnetization curves at T = 310 K of (A) FeHA/Coll25; (B) FeHA/Coll40; and (C) FeHA/Coll50. (Measured curves in black, nonsaturating and saturating paramagnetic contributions, in blue and red respectively.) Insets: small hystereses indicate the paramagnetic nature of the scaffolds.

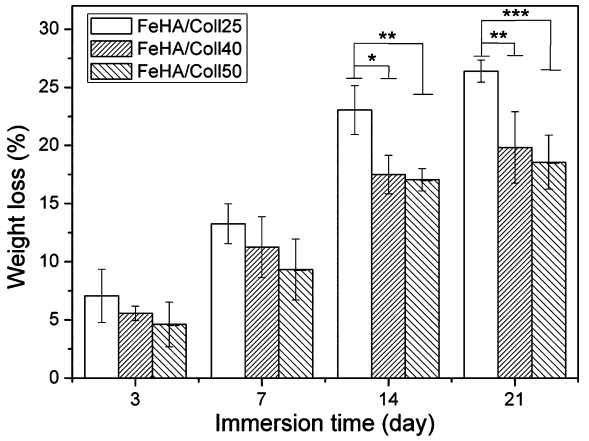

Figure 5. In vitro degradation as a function of time of the FeHA/Coll scaffolds in FBS at 37 °C. *$p \leq 0.05$, **$p \leq 0.01$, ***$p \leq 0.001$.

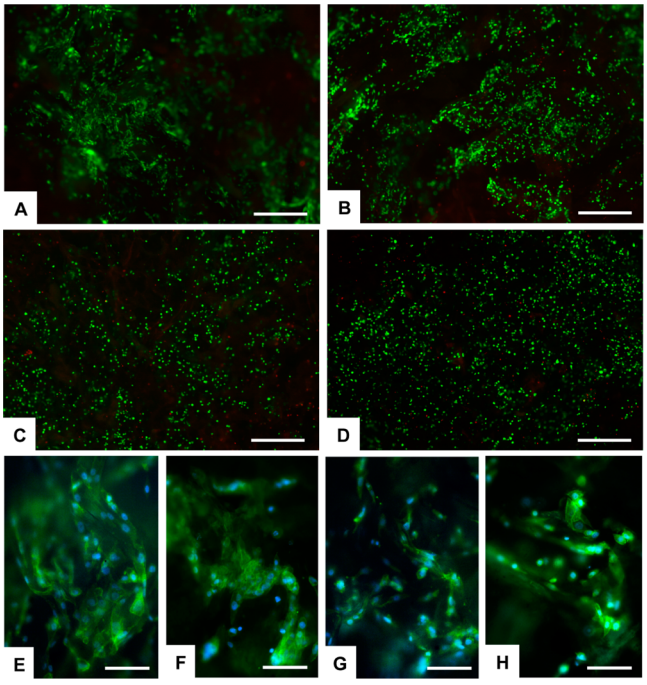

Figure 6. Qualitative analysis of cell viability and morphology. Cell viability was analyzed by the live/dead assay (Calcein AM stains live cells in green, EthD-1 stains dead cells in red). (A–D) HA/Coll, FeHA/Coll25, FeHA/Coll40, and FeHA/Coll50 respectively at day 3. (E–H) Cell morphology analyzed by actin staining at day 7 (actin is shown in green, cell nuclei in blue). Scale bars: (A–D) 500 μm, (E–H) 100 μm.

Coll and FeHA/Coll25 presenting a better performance than FeHA/Coll40 and FeHA/Coll50 (Figure 6A–D). Moreover, the cell morphology, visualized with immunofluorescence, showed good cell adhesion and distribution, exhibiting characteristic osteoblast morphology throughout each scaffold (Figure 6E–H).

For a detailed analysis of cell morphology in the composite scaffolds, SEM characterization has been carried out revealing very high cell integration within the structure of the magnetic scaffolds comparable to the nonmagnetic HA/Coll scaffold, already well tested in previous in vitro and in vivo studies and used in this work as a control scaffold.[56,57] It is worth noticing that cells well exploited the fiber mesh of the composites, indicating cell survival and biocompatible performances of such scaffolds (Figure 2B, E, H, K).

Cell proliferation was evaluated by the MTT assay and results were plotted in a bar graph (Figure 7). The groups of magnetic material showed a high rate of cell proliferation, equal or even higher than that of the control group. FeHA/Coll25 presents better performance than FeHA/Coll40 and FeHA/Coll50 scaffolds, in particular at day 3 when the FeHA/Coll25 achieves the highest value for cell proliferation reaching a plateau ($p \leq 0.05$; $p \leq 0.01$). FeHA/Coll25 scaffold has therefore the potential to strongly enhance cell proliferation at

dx.doi.org/10.1021/am5050967 | ACS Appl. Mater. Interfaces 2014, 6, 15697–15707

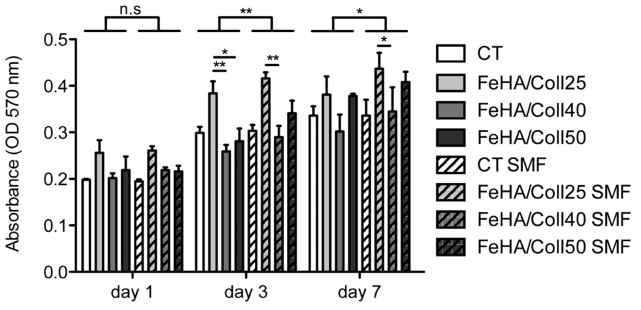

Figure 7. Analysis of cell proliferation by the MTT assay after 1, 3, and 7 days of cell seeding ($n = 3$), either with or without the application of a SMF. (A) Cell proliferation is higher for FeHA/Coll25 composite at day 1 and day 3. (B) Application of a SMF results in an overall increase in cell proliferation. (C) Magnetic scaffolds have the best performance under the application of a SMF. $*p \leq 0.05$, $**p \leq 0.01$.

an early stage, which may be important for future tissue regeneration applications, even though at day 7 no significant difference was seen between the magnetic scaffold groups and the control group.

Overall, both magnetic FeHA/Coll composites show high biocompatibility. The in vitro performance of the magnetic biohybrid composites seems to be affected more by their chemical and morphological features than by their magnetic properties. In fact, the best in vitro performance of FeHA/Coll25 can be assigned, as previously described, to its more open porosity, with respect to the FeHA/Coll40 and FeHA/Coll50 composites, which allows increased cell adhesion and proliferation.

SMF Application. Considering that the main aim of this study is to set up a scaffold that can be magnetized under the application of an external SMF influencing cell behavior and at the same time could selectively attract growth factors linked to magnetic carriers, the MTT experiment was performed also with the application of a 320 mT SMF to address the magnetic properties contribution to the in vitro performance. An overall increase in cell proliferation due to the SMF application was observed. In particular, a statistical significant difference was seen at day 3 ($p \leq 0.01$) and at day 7 ($p \leq 0.05$) (Figure 7). Looking in detail at the behavior of cells seeded into scaffolds under SMF application, we can see that, again, FeHA/Coll25 showed the best performance. In detail, FeHA/Coll25 showed a significantly higher cell proliferation compared to the FeHA/Coll40 (day 3 $p \leq 0.01$; day 7 $p \leq 0.05$).

Due to the encouraging results obtained with FeHA/Coll25 group also with an SMF application, for the gene expression analysis we focused on a comparison between the group FeHA/Coll25 and control HA/Coll. Preliminary gene expression analysis is presented in Figure 8 and the results show an increase in Col1A1, RUNX2, and ALP in cells cultured in the magnetic scaffolds with respect to the nonmagnetic control HA/Coll (1.53-fold, 1.13-fold, and 2.31-fold, respectively). Moreover, the application of SMF increased this difference even further for Col1A1 (2.91-fold) and RUNX2 (2.12-fold).

The above results show that, not only the novel magnetic scaffolds are biocompatible, but moreover, if they are subjected to a SMF application, cell behavior is even improved with respect to the control scaffold, which is already well tested and in clinical use (RegenOss, Fin-Ceramica SpA, Italy).

DISCUSSION

According to Tampieri et al.[35] the unique way to obtain Fe-doped HA endowed with superparamagnetic properties requires the preservation of both Fe^{2+} and Fe^{3+} species to enter in the HA structure in two different coordination positions of Ca. In this work, when the collagen acid suspension was dropped into the basic suspension containing Fe^{2+} and Fe^{3+} ions, Fe-doped HA nanocrystals were nucleated during the collagen fibrillogenesis, taking advantage of the ability of the negatively charged carboxylate groups of collagen to bind Fe and Ca ions that, in turn, are the pinning of FeHA nucleation. The ability of collagen to bind Fe as well as Ca ions is well documented.[49,58] To nucleate magnetic FeHA phase the Fe^{3+}/Fe^{2+} ratio was set up to 2/3 to overcome the oxidation of Fe^{2+}, occurring in basic condition that causes an increase in Fe^{3+} concentration and the imbalance of the Fe^{3+}/Fe^{2+} ratio needed to have a magnetic material.

It was found that the synthesis temperature influences the chemical-physical features of the mineral phase of the hybrid composite scaffolds: in particular, the increase of the synthesis temperature enhanced the degree of crystallinity of the CaP phases (amorphous CaP at 25 °C and apatite at 40 and 50 °C), increased the amount of Fe ions in the Ca positions of the crystal lattice and leaded the formation of low amount of magnetite (only in the case of FeHA/Coll50), influencing the magnetization values of the entire scaffolds, and hence their biological performance. The superparamagnetic properties of the composites are affected by the structural confinement exerted by the protein template on the mineral phase, preventing free crystallization and growth and thus reducing the structural order at lattice level of both incorporated iron species.[35] In fact, the relative magnetization values of the FeHA nucleated on the collagen are lower in comparison to the values

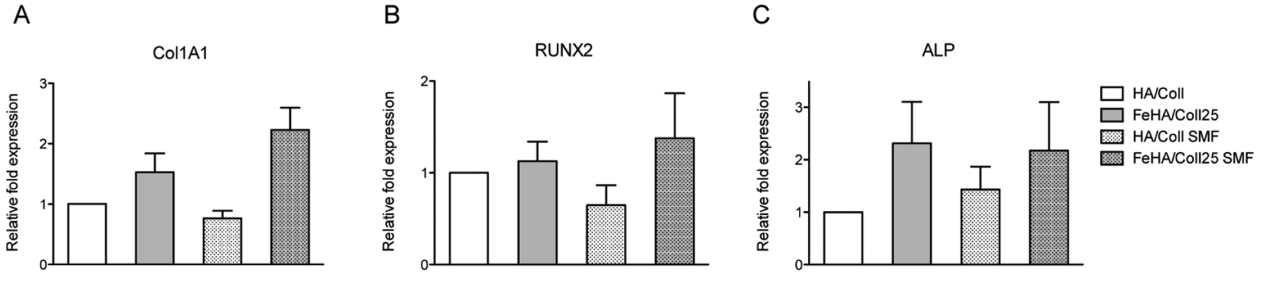

Figure 8. Gene expression analysis. Relative quantification of gene expression after 7 days of MG63 culture in the magnetic scaffold FeHA/Coll25 and respective control HA/Coll, with and without the application of a SMF. Results were normalized to GAPDH and presented as fold change respect to HA/Coll control group. (A) Collagen type I, α-1 (COL1A1). (B) Runt-related transcription factor 2 (RUNX2). (C) Alkaline phosphatase (ALP).

of the pure FeHA synthesized in similar conditions.[36] The high magnetic properties of FeHA/Coll50 in comparison with FeHA/Coll40 cannot be ascribed only to the presence of magnetite, but it can be explained on the basis of an additional contribution due to the formation a new magnetic phase as confirmed by the higher amount of Fe ions incorporated into the apatitic lattice. This phenomenon will be the aim of future studies using peculiar and nonconventional analytical techniques.

Bock et al. transformed scaffolds of HA nucleated on collagen to magnetic scaffolds by dip-coating in aqueous ferrofluids containing iron oxide nanoparticles coated with various biopolymers.[59] The magnetic features of these scaffolds were more pronounced than those of FeHA/Coll; however, in this work, we succeeded to prepare a biomimetic biodegradable magnetic phase to replace the iron oxide phase whose long-term cytotoxic effects in the human body especially caused by its low biodegradation, is becoming an important concern.

It is commonly accepted that the degradation rates of scaffolds for bone tissue engineering must be matched to the rate of various cellular processes in order to optimize tissue regeneration.[60] To avoid a premature degradation FeHA/Coll scaffolds were cross-linked with BDDGE and the in vitro degradation profiles showed good stability for all the materials when they were in contact with the physiological fluid. Actually, in the first 7 days, which is a good time for the cell colonization in vivo, the weight loss of scaffolds was only about the 10%.

In vitro investigations indicated the biocompatibility of the magnetic scaffolds displaying good ability to support cell adhesion and proliferation. The magnetization of the superparamagnetic scaffolds, induced by applying an external SMF improves cell proliferation compared to the nonmagnetic control scaffold. It has to be considered that the final microstructure of the scaffold in terms of open porosity and the degradation rate seem to have great influence on the cell behavior in vitro, as well as the presence of iron into the CaP phase positively influences cell adhesion and proliferation. In fact, these features overcome the detrimental effect due to the low magnetization extent of FeHA/Coll25, in respect to FeHA/Coll40 and FeHA/Coll50.

CONCLUSIONS

The innovative composites prepared in this work can be potentially employed to develop a new class of smart magnetic scaffold able to be magnetized under the application of an external SMF. The magnetic features of the scaffold have been proved to have an activation effect on osteoblast cells controlling the bone growth and improving the whole regenerative process. An extensive physical−chemical, microstructural, and magnetic characterization has been performed as well as in vitro degradation and preliminary biological in vitro tests demonstrating the ability of these scaffolds to support cell adhesion and proliferation and how their performance is enhanced when a SMF is applied. These positive results can stimulate further in vitro and in vivo investigations on the potential application of these bioinspired magnetic scaffolds to trigger and direct osteogenesis, and to repair large bone defects through a magnetic remote control tuning the regenerative process. Moreover, growth factors and/or other key biomolecules linked to magnetic carriers could be selectively attracted toward and within the hybrid scaffold when magnetized. The magnetic behavior of the FeHA directly nucleated on the collagen can also allow to label the scaffold to be visualized in vivo by MRI.

ASSOCIATED CONTENT

Supporting Information

Experimental details of TEM analyses and cell−material interaction of HA/Coll and FeHA/Coll scaffolds. DCS curves of HA/Coll and FeHA/Coll scaffolds. This material is available free of charge via the Internet at http://pubs.acs.org.

AUTHOR INFORMATION

Corresponding Author

*Email: anna.tampieri@istec.cnr.it.

Notes

The authors declare no competing financial interest.

ACKNOWLEDGMENTS

This work was supported by the EU projects "MAGISTER" NMP3-LA-2008-214685 and "SMILEY" NMP-2012-SMALL-6-310637. We thank Dr. Teresa D'Alessandro for the experimental part.

REFERENCES

(1) McCullen, S. D.; Chow, A. G.; Stevens, M. M. In Vivo Tissue Engineering of Musculoskeletal Tissues. *Curr. Opin. Biotechnol.* **2011**, *22*, 715−20.

(2) Panseri, S.; Russo, A.; Cunha, C.; Bondi, A.; Di Martino, A.; Patella, S.; Kon, E. Osteochondral Tissue Engineering Approaches for Articular Cartilage and Subchondral Bone Regeneration. *Knee Surg. Sports Traumatol. Arthrosc.* **2012**, *20*, 1182−91.

(3) Arinzeh, T. L.; Tran, T.; McAlary, J.; Daculsi, G. A Comparative Study of Biphasic Calcium Phosphate Ceramics for Human Mesenchymal Stem-Cell-Induced Bone Formation. *Biomaterials* **2005**, *26*, 3631−8.

(4) Cheng, L.; Ye, F.; Yang, R.; Lu, X.; Shi, Y.; Li, L.; Fan, H.; Bu, H. Osteoinduction of Hydroxyapatite/β-Tricalcium Phosphate Bioceramics in Mice with a Fractured Fibula. *Acta Biomater.* **2010**, *6*, 1569−1574.

(5) Gómez-Morales, J.; Iafisco, M.; Delgado-López, J. M.; Sarda, S.; Drouet, C. Progress on the Preparation of Nanocrystalline Apatites and Surface Characterization: Overview of Fundamental and Applied Aspects. *Prog. Cryst. Growth Charact. Mater.* **2013**, *59*, 1−46.

(6) Hutchens, S. A.; Benson, R. S.; Evans, B. R.; O'Neill, H. M.; Rawn, C. J. Biomimetic Synthesis of Calcium-Deficient Hydroxyapatite in a Natural Hydrogel. *Biomaterials* **2006**, *27*, 4661−4670.

(7) Tampieri, A.; Celotti, G.; Landi, E.; Sandri, M.; Roveri, N.; Falini, G. Biologically Inspired Synthesis of Bone-like Composite: Self-assembled Collagen Fibers/Hydroxyapatite nanocrystals. *J. Biomed. Mater. Res., Part A* **2003**, *67*, 618−625.

(8) Tampieri, A.; Sandri, M.; Landi, E.; Pressato, D.; Francioli, S.; Quarto, R.; Martin, I. Design of Graded Biomimetic Osteochondral Composite Scaffolds. *Biomaterials* **2008**, *29*, 3539−3546.

(9) Zhao, H.; Wang, G.; Hu, S.; Cui, J.; Ren, N.; Liu, D.; Liu, H.; Cao, C.; Wang, J.; Wang, Z. In Vitro Biomimetic Construction of Hydroxyapatite-Porcine Acellular Dermal Matrix Composite Scaffold for MC3T3-E1 Preosteoblast Culture. *Tissue Eng., Part A* **2011**, *17*, 765−776.

(10) Bernhardt, A.; Lode, A.; Boxberger, S.; Pompe, W.; Gelinsky, M. Mineralized Collagen—An Artificial, Extracellular Bone Matrix-Improves Osteogenic Differentiation of Bone Marrow Stromal Cells. *J. Mater. Sci.: Mater. Med.* **2008**, *19*, 269−275.

(11) Domaschke, H.; Gelinsky, M.; Burmeister, B.; Fleig, R.; Hanke, T.; Reinstorf, A.; Pompe, W.; Rösen-Wolff, A. In Vitro Ossification and Remodeling of Mineralized Collagen I Scaffolds. *Tissue Eng.* **2006**, *12*, 949−958.

(12) Rhee, S.-H.; Lee, J. D.; Tanaka, J. Nucleation of Hydroxyapatite Crystal through Chemical Interaction with Collagen. *J. Am. Ceram. Soc.* **2000**, *83*, 2890−2892.
(13) Amini, A. R.; Laurencin, C. T.; Nukavarapu, S. P. Bone Tissue Engineering: Recent Advances and Challenges. *CRC Crit. Rev. Bioeng.* **2012**, *40*, 363−408.
(14) Kanczler, J. M.; Oreffo, R. O. C. Osteogenesis and Angiogenesis: The Potential for Engineering Bone. *Eur. Cells Mater.* **2008**, *15*, 100−114.
(15) Lee, K.; Silva, E. A.; Mooney, D. J. Growth Factor Delivery-Based Tissue Engineering: General Approaches and a Review of Recent Developments. *J. R. Soc., Interface* **2011**, *8*, 153−170.
(16) Grace, K. L. R.; Revell, W. J.; Brookes, M. The Effects of Pulsed Electromagnetism on Fresh Fracture Healing: Osteochondral Repair in the Rat Femoral Groove. *Orthopedics* **1998**, *21*, 297−302.
(17) Glazer, P. A.; Heilmann, M. R.; Lotz, J. C.; Bradford, D. S. Use of Electromagnetic Fields in a Spinal Fusion: A Rabbit Model. *Spine* **1997**, *22*, 2351−2356.
(18) Yan, Q. C.; Tomita, N.; Ikada, Y. Effects of Static Magnetic Field on Bone Formation of Rat Femurs. *Med. Eng. Phys.* **1998**, *20*, 397−402.
(19) Assiotis, A.; Sachinis, N. P.; Chalidis, B. E. Pulsed Electromagnetic Fields for the Treatment of Tibial Delayed Unions and Nonunions. A Prospective Clinical Study and Review of the Literature. *J. Orthop. Sur. Res.* **2012**, *7*, 24.
(20) Chalidis, B.; Sachinis, N.; Assiotis, A.; Maccauro, G. Stimulation of Bone Formation and Fracture Healing with Pulsed Electromagnetic Fields: Biologic Responses and Clinical Implications. *Int. J. Immunopathol. Pharmacol.* **2011**, *24*, 17−20.
(21) Torbet, J.; Ronziere, M. C. Magnetic Alignment of Collagen During Self-Assembly. *Biochem. J.* **1984**, *219*, 1057−1059.
(22) Higashi, T.; Yamagishi, A.; Takeuchi, T.; Kawaguchi, N.; Sagawa, S.; Onishi, S.; Date, M. Orientation of Erythrocytes in a Strong Static Magnetic Field. *Blood* **1993**, *82*, 1328−1334.
(23) Kotani, H.; Kawaguchi, H.; Shimoaka, T.; Iwasaka, M.; Ueno, S.; Ozawa, H.; Nakamura, K.; Hoshi, K. Strong Static Magnetic Field Stimulates Bone Formation to a Definite Orientation In Vitro and In Vivo. *J. Bone Miner. Res.* **2002**, *17*, 1814−1821.
(24) Xu, H.-Y.; Gu, N. Magnetic Responsive Scaffolds and Magnetic Fields in Bone Repair and Regeneration. *Front. Mater. Sci.* **2014**, *8*, 20−31.
(25) Yao, W.; Wen, J.; Xiantao, W.; Bin, H.; Xiaobo, Z.; Gang, W.; Zhongwei, G. A Novel Calcium Phosphate Ceramic−Magnetic Nanoparticle Composite as a Potential Bone Substitute. *Biomed. Mater.* **2010**, *5*, 015001.
(26) Panseri, S.; Cunha, C.; D'Alessandro, T.; Sandri, M.; Russo, A.; Giavaresi, G.; Marcacci, M.; Hung, C. T.; Tampieri, A. Magnetic Hydroxyapatite Bone Substitutes to Enhance Tissue Regeneration: Evaluation In Vitro Using Osteoblast-Like Cells and In Vivo in a Bone Defect. *PLoS One* **2012**, *7*, e38710.
(27) Meng, J.; Xiao, B.; Zhang, Y.; Liu, J.; Xue, H.; Lei, J.; Kong, H.; Huang, Y.; Jin, Z.; Gu, N.; Xu, H. Super-Paramagnetic Responsive Nanofibrous Scaffolds Under Static Magnetic Field Enhance Osteogenesis for Bone Repair In Vivo. *Sci. Rep.* **2013**, *3*, 2655.
(28) Panseri, S.; Russo, A.; Sartori, M.; Giavaresi, G.; Sandri, M.; Fini, M.; Maltarello, M. C.; Shelyakova, T.; Ortolani, A.; Visani, A.; Dediu, V.; Tampieri, A.; Marcacci, M. Modifying Bone Scaffold Architecture In Vivo with Permanent Magnets to Facilitate Fixation of Magnetic Scaffolds. *Bone* **2013**, *56*, 432−439.
(29) Shan, D.; Shi, Y.; Duan, S.; Wei, Y.; Cai, Q.; Yang, X. Electrospun Magnetic Poly(L-lactide) (PLLA) Nanofibers by Incorporating PLLA-Stabilized Fe_3O_4 Nanoparticles. *Mater. Sci. Eng., C* **2013**, *33*, 3498−3505.
(30) Meng, J.; Zhang, Y.; Qi, X.; Kong, H.; Wang, C.; Xu, Z.; Xie, S.; Gu, N.; Xu, H. Paramagnetic Nanofibrous Composite Films Enhance the Osteogenic Responses of Pre-Osteoblast Cells. *Nanoscale* **2010**, *2*, 2565−2569.
(31) Hou, R.; Zhang, G.; Du, G.; Zhan, D.; Cong, Y.; Cheng, Y.; Fu, J. Magnetic Nanohydroxyapatite/PVA Composite Hydrogels for Promoted Osteoblast Adhesion and Proliferation. *Colloids Surf., B* **2013**, *103*, 318−325.
(32) Mertens, M. E.; Hermann, A.; Bühren, A.; Olde-Damink, L.; Möckel, D.; Gremse, F.; Ehling, J.; Kiessling, F.; Lammers, T. Iron Oxide-Labeled Collagen Scaffolds for Non-Invasive MR Imaging in Tissue Engineering. *Adv. Funct. Mater.* **2014**, *24*, 754−762.
(33) Almeida, J. P. M.; Chen, A. L.; Foster, A.; Drezek, R. In Vivo Biodistribution of Nanoparticles. *Nanomedicine (London, U.K.)* **2011**, *6*, 815−835.
(34) Mahmoudi, M.; Hofmann, H.; Rothen-Rutishauser, B.; Petri-Fink, A. Assessing the In Vitro and In Vivo Toxicity of Superparamagnetic Iron Oxide Nanoparticles. *Chem. Rev. (Washington, DC, U.S.)* **2012**, *112*, 2323−2338.
(35) Tampieri, A.; D'Alessandro, T.; Sandri, M.; Sprio, S.; Landi, E.; Bertinetti, L.; Panseri, S.; Pepponi, G.; Goettlicher, J.; Bañobre-López, M.; Rivas, J. Intrinsic Magnetism and Hyperthermia in Bioactive Fe-Doped Hydroxyapatite. *Acta Biomater.* **2012**, *8*, 843−851.
(36) Panseri, S.; Cunha, C.; D'Alessandro, T.; Sandri, M.; Giavaresi, G.; Marcacci, M.; Hung, C. T.; Tampieri, A. Intrinsically Superparamagnetic Fe-Hydroxyapatite Nanoparticles Positively Influence Osteoblast-Like Cell Behavior. *J. Nanobiotechnol.* **2012**, *10*, 32.
(37) Bañobre-López, M.; Piñeiro-Redondo, Y.; De Santis, R.; Gloria, A.; Ambrosio, L.; Tampieri, A.; Dediu, V.; Rivas, J. Poly(caprolactone) Based Magnetic Scaffolds for Bone Tissue Engineering. *J. Appl. Phys. (Melville, NY, U.S.)* **2011**, *109*, 07B313.
(38) Gloria, A.; Russo, T.; D'Amora, U.; Zeppetelli, S.; D'Alessandro, T.; Sandri, M.; Bañobre-López, M.; Piñeiro-Redondo, Y.; Uhlarz, M.; Tampieri, A.; Rivas, J.; Herrmannsdörfer, T.; Dediu, V. A.; Ambrosio, L.; De Santis, R. Magnetic Poly(ε-caprolactone)/Iron-Doped Hydroxyapatite Nanocomposite Substrates for Advanced Bone Tissue Engineering. *J. R. Soc., Interface* **2013**, *10*, 20120833.
(39) Iafisco, M.; Sandri, M.; Panseri, S.; Delgado-López, J. M.; Gómez-Morales, J.; Tampieri, A. Magnetic Bioactive and Biodegradable Hollow Fe-Doped Hydroxyapatite Coated Poly(L-lactic) Acid Micro−Nanospheres. *Chem. Mater.* **2013**, *25*, 2610−2617.
(40) Tampieri, A.; Sprio, S.; Sandri, M.; Valentini, F. Mimicking Natural Bio-Mineralization Processes: A New Tool for Osteochondral Scaffold Development. *Trends Biotechnol.* **2011**, *29*, 526−535.
(41) Tzaphlidou, M.; Fountos, G.; Glaros, D. Bone Hydroxyapatite/Collagen Ratio: In Vivo Measurements by X-ray Absorptiometry. *Ann. N.Y. Acad. Sci.* **2000**, *904*, 284−286.
(42) Nicoletti, A.; Fiorini, M.; Paolillo, J.; Dolcini, L.; Sandri, M.; Pressato, D. Effects of Different Crosslinking Conditions on the Chemical−Physical Properties of a Novel Bio-Inspired Composite Scaffold Stabilized with 1,4-Butanediol Diglycidyl Ether (BDDGE). *J. Mater. Sci: Mater. Med.* **2013**, *24*, 17−35.
(43) Dorozhkin, S. V. Amorphous Calcium (Ortho)Phosphates. *Acta Biomater.* **2010**, *6*, 4457−4475.
(44) Iafisco, M.; Ruffini, A.; Adamiano, A.; Sprio, S.; Tampieri, A. Biomimetic Magnesium−Carbonate−Apatite Nanocrystals Endowed with Strontium Ions as Anti-Osteoporotic Trigger. *Mater. Sci. Eng., C* **2014**, *35*, 212−219.
(45) Perales Perez, O.; Umetsu, Y.; Sasaki, H. Precipitation and Densification of Magnetic Iron Compounds from Aqueous Solutions at Room Temperature. *Hydrometallurgy* **1998**, *50*, 223−242.
(46) Mu, C.; Li, D.; Lin, W.; Ding, Y.; Zhang, G. Temperature Induced Denaturation of Collagen in Acidic Solution. *Biopolymers* **2007**, *86*, 282−287.
(47) Leikin, S.; Rau, D. C.; Parsegian, V. A. Temperature-Favored Assembly of Collagen is Driven by Hydrophilic not Hydrophobic Interactions. *Nat. Struct. Biol.* **1995**, *2*, 205−210.
(48) Delgado-López, J. M.; Iafisco, M.; Rodríguez, I.; Tampieri, A.; Prat, M.; Gómez-Morales, J. Crystallization of Bioinspired Citrate-Functionalized Nanoapatite with Tailored Carbonate Content. *Acta Biomater.* **2012**, *8*, 3491−3499.
(49) Chen, F.; Fan, D. Investigation on the Interaction Between Human-Like Collagen and Iron. *Adv. Mater. Res. (Durnten-Zurich, Switz.)* **2011**, *287*−*290*, 2941−2944.

(50) Zeugolis, D. I.; Raghunath, M. The Physiological Relevance of Wet Versus Dry Differential Scanning Calorimetry for Biomaterial Evaluation: A Technical Note. *Polym. Int.* **2010**, *59*, 1403−1407.
(51) Meng, L.; Arnoult, O.; Smith, M.; Wnek, G. E. Electrospinning of in Situ Crosslinked Collagen Nanofibers. *J. Mater. Chem.* **2012**, *22*, 19412−19417.
(52) Williams, D. B.; Carter, C. B. *Transmission Electron Microscopy: A Textbook for Materials Science*; Springer: New York, 2009; Ch. 1, p717.
(53) Gómez-Morales, J.; Delgado-López, J. M.; Iafisco, M.; Hernández-Hernández, A.; Prat, M. Amino Acidic Control of Calcium Phosphate Precipitation by Using the Vapor Diffusion Method in Microdroplets. *Cryst. Growth Des.* **2011**, *11*, 4802−4809.
(54) Combes, C.; Rey, C. Amorphous Calcium Phosphates: Synthesis, Properties and Uses in Biomaterials. *Acta Biomater.* **2010**, *6*, 3362−3378.
(55) Grover, C. N.; Cameron, R. E.; Best, S. M. Investigating the Morphological, Mechanical, and Degradation Properties of Scaffolds Comprising Collagen, Gelatin, and Elastin for Use in Soft Tissue Engineering. *J. Mech. Behav. Biomed. Mater.* **2012**, *10*, 62−74.
(56) Scaglione, S.; Giannoni, P.; Bianchini, P.; Sandri, M.; Marotta, R.; Firpo, G.; Valbusa, U.; Tampieri, A.; Diaspro, A.; Bianco, P.; Quarto, R. Order Versus Disorder: In Vivo Bone Formation Within Osteoconductive Scaffolds. *Sci. Rep.* **2012**, *2*, 274.
(57) Tampieri, A.; Celotti, G.; Landi, E. From Biomimetic Apatites to Biologically Inspired Composites. *Anal. Bioanal. Chem.* **2005**, *381*, 568−576.
(58) Landis, W.; Jacquet, R. Association of Calcium and Phosphate Ions with Collagen in the Mineralization of Vertebrate Tissues. *Calcif. Tissue Int.* **2013**, *93*, 329−337.
(59) Bock, N.; Riminucci, A.; Dionigi, C.; Russo, A.; Tampieri, A.; Landi, E.; Goranov, V. A.; Marcacci, M.; Dediu, V. A Novel Route in Bone Tissue Engineering: Magnetic Biomimetic Scaffolds. *Acta Biomater.* **2010**, *6*, 786−796.
(60) Lee, K. Y.; Mooney, D. J. Hydrogels for Tissue Engineering. *Chem. Rev. (Washington, DC, U.S.)* **2001**, *101*, 1869−1880.